Bulletin of the Seismological Society of America, Vol. 108, No. 2, pp. 742–760, April 2018, doi: 10.1785/0120170171

Ⓔ

An Analytical Effective Point-Source-Based Distance-Conversion Approach to Mimic the Effects of Extended Faults on Seismic Hazard Assessment

by Behrooz Tavakoli, Farhad Sedaghati,* and Shahram Pezeshk

Abstract An analytical point-source-based approach is presented to convert the Joyner–Boore (R_{JB}) distance to various source-to-site distance metrics for a given tectonic region. The analytical-based approach is combined with the effects of the region-specific propagation path to define a new effective distance-conversion equation for use in ground-motion simulations and the existing stochastic-based ground-motion prediction equations (GMPEs), in which the effect of extended-fault rupture on the ground motions is ignored. The proposed region-specific distance-conversion approach may also be used to capture the effect of extended-fault sources on ground-motion amplitudes in the probabilistic seismic hazard analysis (PSHA) studies in which earthquake occurrences are modeled as point-source models. In this approach, virtual sites are defined on a bathtub-shaped surface around an extended-fault source on which all sites have identical R_{JB} distances. The source-to-site distances are analytically derived using the law of sines and cosines. The distance-conversion process is then combined with region-specific geometrical spreading and attenuation functions to improve and adjust the point-source distance metrics into new effective epicentral distance or hypocentral distance metrics, and to mimic the effect of extended-fault sources at close distances.

A general effective point-source-based distance-conversion equation is developed in this study, which can be employed for any arbitrary input parameters and functions, such as the relations between the fault dimensions and magnitude, location of the fault with respect to virtual sites, probability distribution of focal depths, and geometrical spreading and anelastic attenuation functions corresponding to the region under study. As an application for the hazard analysis, a simple PSHA study is performed within a circular areal source zone using a published R_{RUP}-based GMPE and the source-to-site distance-conversion equations developed in this study to demonstrate the effect of using inconsistent source-to-site distance metrics on the seismic hazard curves at a given site.

Electronic Supplement: Tabular data and MATLAB code to estimate the effective hypocentral and epicentral distances.

Introduction

The Joyner–Boore distance (the closest distance to the surface projection of an extended fault, R_{JB}) or rupture distance (the closest distance to an extended fault, R_{RUP}) are commonly used in ground-motion prediction equations (GMPEs) to capture the effect of finite-fault ruptures, particularly for near-source recordings. In probabilistic seismic hazard analysis (PSHA), the spatial distribution of earthquakes within a large areal seismic source, where the traces of faults are unknown, is described by associating them with point-source models. Therefore, it is necessary to convert the point-source-based distance measures such as epicentral (R_{EPI}) or hypocentral (R_{HYP}) distances into the extended fault-based distance metrics defined in GMPEs for use in PSHA. In other words, in the PSHA integrals, each potential event has a distance R_{EPI} from the site, but to predict ground

*Now at AON Benfield, Analytics, Impact Forecasting, 200 E Randolph, 10th floor, Chicago, Illinois 60601; farhad.sedaghati@aonbenfield.com.

motions for that event, the R_{EPI} must be converted into an R_{JB} for that event, and the adjusted R_{JB} is then used in the extended fault-based GMPE to estimate ground-motion amplitudes. Various methods have been proposed to convert point-source distance metrics into extended-fault source distance metrics and vice versa.

Scherbaum *et al.* (2004) developed the empirical distance-conversion relations for three types of generic, strike-slip, and all dipping fault scenarios using simulated fault ruptures and observation points around the faults. In the Scherbaum *et al.* (2004) approach, the extended-fault rupture scenarios are generated based on the magnitude, the selected dip angle, and the hypocenter location on the fault rupture, which is randomly chosen from a truncated normal distribution. Then, the observation points for the simulated extended fault are randomly and uniformly chosen between 0° and 360° about the fault rupture to calculate various distance measures (e.g., R_{EPI} from the site) with respect to R_{JB} distance and earthquake magnitude. Because the R_{JB} distance is always smaller than or equal to other distance measures, the positive residuals between various measures of distance and R_{JB} distance are used to determine the distance-conversion relations. To this end, polynomial functional forms are provided to estimate the mean converted distance metrics as well as their standard errors by fitting a gamma probability distribution function to residuals, which are defined as the difference between the R_{JB} distance and R_{EPI} or R_{HYP} distances. This simulation-based approach calculates the converted R_{EPI} or R_{HYP} distances for a given R_{JB} distance by ignoring the effect of wave propagation path from each portion of the entire fault to the site. The wave propagation path affects the mean converted distance, particularly for large fault ruptures by assigning nonuniform weighting factors (e.g., $R^{-\gamma}$ propagation decay, in which γ is the geometrical spreading exponent) to source-to-site distances. The Scherbaum *et al.* (2004) approach predicts large values of other distance measures near the fault ruptures, such as R_{EPI}, for an initial-fixed value of R_{JB}, compared with those approaches that involve GMPEs in the process of averaging possible epicenter or hypocenter distances (e.g., Electric Power Research Institute [EPRI], 2004). Therefore, the direct use of these distance-conversion relations may not be considered suitable for evaluating ground-motion amplitudes, particularly for the areal seismic source models used in PSHA studies.

EPRI (2004) used GMPEs developed for central and eastern United States (CEUS) to provide the empirical point-source distance-conversion equations for various measures of distance defined in the CEUS GMPEs. These distance-conversion equations are used to adjust various source-to-site distances in areal seismic sources with unknown traces of faulting for PSHA studies in the CEUS. In the EPRI (2004) approach, unknown extended-fault ruptures within a given areal seismic source are modeled to be an equal combination of vertical strike-slip faults and 40° dip reverse faults, with uniform random orientations distributed in azimuth from 0° to 360° about the earthquake epicenter and with uniform random depth constrained to a maximum depth of 25 km. Then, the two most widely used distances, the R_{JB} distance and the R_{RUP} distance, are calculated using an appropriate geometry for each randomly simulated fault rupture about the earthquake with moment magnitude of **M** and epicentral distance of R_{EPI} from the site. Because seismic energy is released from the entire extended-fault rupture during a large earthquake, R_{JB} or R_{RUP} distances are used in appropriate R_{JB}- or R_{RUP}-based GMPEs to compute the geometric-mean ground-motion intensity measure (GMIM) of interest, such as peak ground acceleration as a measure of energy intensity of shaking for both strike-slip or reverse-fault rupture models. The expected geometric-mean GMIM is used in those corresponding GMPEs to backcalculate the appropriate average R_{JB} or R_{RUP} distance and associated uncertainties with respect to the GMIM of interest. The EPRI (2004) distance-conversion relations may be sensitive to the selection of GMPEs and the frequency of ground motions. These GMPE-based conversion equations also need to be modified for areal seismic sources where a preferred fault orientation or explicit modeling of finite ruptures is warranted.

The U.S. Geological Survey (USGS) distance-conversion approach used in the USGS hazard maps for the CEUS (Petersen *et al.*, 2008) assumes that seismic energy is released from the earthquake epicenter rather than the crust around the entire fault rupture during a large earthquake. In the USGS hazard maps, areal seismic source models are defined to account for future random earthquakes in areas with little or no historical seismicity for the PSHA study. Within areal source zones, a virtual vertical strike-slip fault is defined for each grid cell of source zones, and the fault rupture is located on the center of each grid cell. The fault strike is randomly oriented in azimuth from 0° to 360° about the earthquake epicenter, and the mean R_{JB} distance is calculated for a fixed R_{EPI} distance using the law of sines and cosines. The dimension of a fault rupture varies for each magnitude increment and is obtained from the Wells and Coppersmith (1994) empirical relationships. The USGS distance-conversion relationships are only applicable for vertical fault ruptures and may not be used for dipping fault ruptures and the regions with various geologic structures.

Bommer and Akkar (2012) suggested to directly develop pairs of GMPEs for both point- and extended-source distance measures from the same ground-motion dataset. They performed a simple PSHA study and demonstrated that GMIMs obtained from the R_{JB}-based ground-motion models relative to R_{EPI}-based ground-motion models underestimate the hazard for areal seismic sources. The current GMPEs developed for the United States have often used the R_{JB} or R_{RUP} distances from extended-fault sources of moderate-to-large magnitude earthquakes. To use these extended fault-based GMPEs for the case of areal seismic sources within the low-to-moderate seismicity region, which tend to dominate hazard models in a PSHA study, the point-source distances

(R_{EPI} or R_{HYP}) should be converted into the extended-fault distances to adjust distances in the extended fault-based GMPEs if the point-source-based GMPE models are not available.

The objective of this study is to develop an analytical-based approach to adjust the distance measures defined for the extended-fault source-based GMPEs based on various point-source-based distance metrics for use in the PSHA studies and stochastic ground-motion simulations. The analytical-based approach can be used directly to adjust distances in current extended-fault source-based GMPEs that are developed based on real recorded data. For existing stochastic-based GMPEs in which the effect of extended-fault sources is ignored, and for developing new point-source-based GMPE models, the analytical-based approach developed in this study can be combined with the effects of the region-specific propagation path to define a new effective distance (R_{EFF}) to adjust distances in such GMPEs. The R_{EFF} distance is the distance between a given virtual site and an equivalent point source on a fault that can substitute the extended-fault rupture with a point source and mimic its characteristic. This distance metric is defined in such a way that the seismic energy intensity provided at the given site from the equivalent point source is identical to the energy intensity provided from the extended-fault rupture during a large earthquake.

The USGS and EPRI approaches use the R_{EPI} distance as a reference distance metric and the R_{JB} distance as a target distance metric to link for two distance metrics between a point source and an extended-fault source. In contrast with the EPRI and USGS approaches, we define Joyner–Boore (JB) surfaces containing virtual sites on a bathtub shape with identical R_{JB} distances around an extended-fault source as a reference distance and then analytically derive the average R_{EPI} and R_{HYP} using the law of sines and cosines.

In this study, instead of using virtual faults, which are randomly oriented about a fixed earthquake epicenter (e.g., USGS and EPRI approaches), virtual sites with a constant R_{JB} distance are taken around a fixed fault to improve the computational efficiency in the hazard models. The averaging distance-conversion process is combined with region-specific geometrical spreading and anelastic attenuation functions following the Boore (2009) approach to assign a suitable weighting factor for distance conversion and to adjust the resultant point-source distance metrics into new effective R_{EPI} or R_{HYP} distance metrics that may be entered in current extended-fault source-based GMPEs to adjust the distances for use in the PSHA studies as well as in stochastic ground-motion simulations.

The analytical-based distance-conversion equations developed in this study are generic and can be used for any arbitrary input parameters and functions, such as the empirical relations between fault dimensions and magnitude, location of the fault with respect to virtual sites, fault dips, fault strikes, and probability distribution of focal depths. The proposed approach is able to model the effects of the region-specific propagation path on seismic waves along the desired range of strikes and dip angles from available information about the tectonic region, which are not accounted for in the other available methods.

As an implementation in the seismic hazard assessment, a simple PSHA study is performed within a circular areal source zone associated with both low- and high-seismicity scenarios using a suite of published R_{RUP}-based GMPEs to demonstrate the effect of using inconsistent source-to-site distance metrics on hazard curves at a given site.

General Distance-Conversion Equations

The R_{JB} distance is chosen as the primary reference metric in this study and the other distance matrices are converted as target distance metrics using the law of sines and cosines. The general distance-conversion equations are analytically derived for both vertical and dipping fault rupture scenarios. The analytical-based distance-conversion approach developed in this study has two different aspects compared with the USGS approach.

First, the proposed analytical-based approach is obtained based on positioning virtual sites around an arbitrary fault rupture, whereas the USGS approach simulates random-oriented vertical fault ruptures for a given site to obtain distance-conversion equations. In essence, the distance-conversion results should be insensitive, either if the site is constant and the fault rotates around the center of the fault (virtual faults model) or if the fault is constant and the site rotates around the fault (virtual sites model). However, using the model of virtual sites would improve the computational efficiency in the hazard analysis.

Second, the USGS approach fixes the epicentral distance on the center of fault and then derives the distance-conversion equations to obtain the average R_{JB} distance. On the other hand, in the proposed analytical-based approach, the R_{JB} distance is fixed, and then the distance-conversion equations are derived for various distance metrics. The advantage of using a fixed R_{JB} distance for a known fault and a given azimuth is that there is only one station for an R_{JB} distance, but the station for a fixed epicentral distance can be moved, based on the location of epicenter. Because of this difficulty, the USGS approach limits itself by assuming that the epicenter is always in the center of the fault.

The JB surface has a significant advantage that allows us to choose directly the R_{JB} distance defined in the R_{JB}-based GMPEs as the primary reference metric to convert to all other distance metrics. Figure 1 shows the JB surface about a vertical strike-slip fault and earthquake hypocenter locations, which are dependent on the moment magnitude and are defined by a truncated normal distribution. The location of possible observation points (virtual sites) having the same R_{JB} distances from an extended fault with a vertical dip angle is modeled with two semicircles with radius of R_{JB} at the end points of the fault and two straight lines parallel to the fault. All the virtual sites on this bathtub-shaped JB surface have an

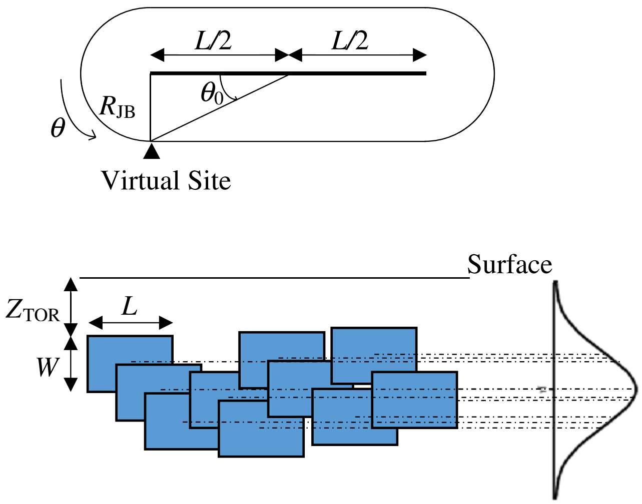

Figure 1. (Top) Joyner–Boore (JB) surface for a vertical strike-slip fault. The line in the middle of the JB surface is the fault length of L. The triangle is the locations of possible observation points (sites or stations) having the same R_{JB} distances from the extended fault. (Bottom) The earthquake hypocenter locations are defined by a truncated normal distribution; however, any probability density function of the hypocenter (e.g., Weibull distribution), in which the hypocenter is weighted toward the bottom of the fault, not centered can be used in the distance-conversion approach. The color version of this figure is available only in the electronic edition.

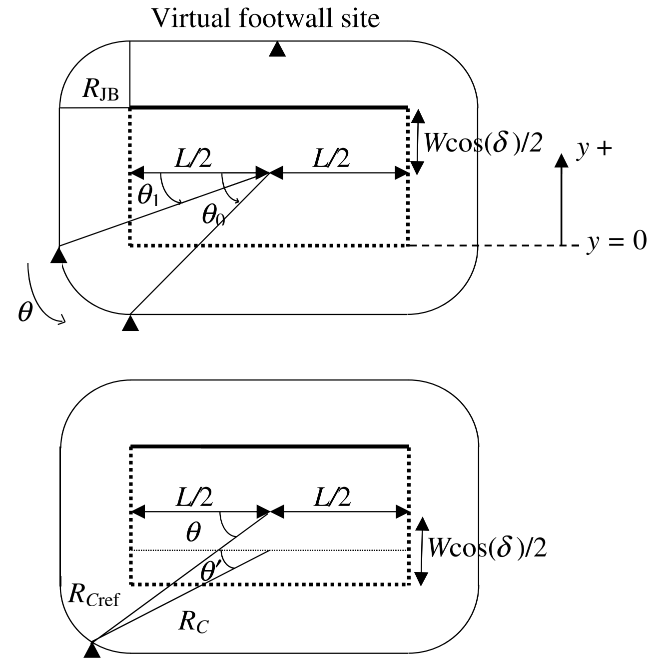

Virtual hanging wall site for the case $\theta_1 < \theta < \theta_0$

Figure 2. JB surface for a dipping fault. The rectangular inside is the fault projection on the surface. The triangles are the locations of possible observation points (sites or stations) having the same R_{JB} distances from the extended fault.

identical R_{JB} distance to the fault. In this figure, the parameter θ_0 is defined as the angle between the fault trace and the line that connects the center of the fault to the intersection of the parallel lines to the fault trace and semicircles (see Fig. 1). The JB surface becomes more complicated for dipping faults because there is a surface projection for the width of the fault. Figure 2 shows the JB surface around a dipping fault. For an extended fault with a width of W and a dip angle of δ, the surface projection of the fault has a width of $W\cos(\delta)$. In this case, the location of possible observation points having the same R_{JB} distances is modeled with four quarter-circles with radius R_{JB} and two parallel lines along the fault length and two parallel lines to the width projection on the ground surface. All the observation points on this JB surface have an identical R_{JB} distance to the fault surface projection.

In Figure 2, the parameter of θ_0 is defined as the angle between the line passing the center of the fault projection in the fault direction and the line that connects the center of the fault projection to the intersection of the parallel lines to the fault length and quarter-circles. The parameter of θ_1 is defined as the angle between the line passing the center of the fault projection in the fault direction and the line that connects the center of the fault projection to the intersection of the parallel lines to the fault width projection and quarter-circles.

Vertical Strike-Slip Faults

Suppose that we have an arbitrary extended-fault rupture produced by a given earthquake and observation points (virtual sites) with a constant R_{JB} distance of interest (see Fig. 1) on the JB surface. We begin with a relationship between R_{JB} and R_{HYP}, which is controlled by the depth of the earthquake as a function of moment magnitude, and the influence of the depth is decreased with increasing distance.

For each observation point with a particular azimuth (θ), the geometry relation between R_{JB} distance and R_{HYP} distance using the law of sines and cosines is expressed by the following equation:

$$< R_{\mathrm{HYP}} >_\theta = \int_{Z_{\mathrm{TOR}}}^{Z_{\mathrm{TOR}}+W} \int_{-L/2}^{L/2} \sqrt{[(R_C^2 + x^2 - 2xR_C\cos(\theta)) + z^2]}\,p(x)p(z)dxdz, \quad (1)$$

in which $< R_{\mathrm{HYP}} >_\theta$ is the mean R_{HYP} distance for a particular θ, and R_C is an auxiliary distance between the center of the fault and the observation point, which is defined as

$$R_C = \begin{cases} \sqrt{(L/2)^2 + R_{\mathrm{JB}}^2 - 2(L/2)R_{\mathrm{JB}}\cos\left[180 - \left(\theta + \arcsin\left(\frac{\sin(\theta)L/2}{R_{\mathrm{JB}}}\right)\right)\right]} & \text{if } 0 \le \theta < \theta_0 \\ R_{\mathrm{JB}}/\sin(\theta) & \text{if } \theta_0 \le \theta < 90, \end{cases} \tag{2}$$

in which $\theta_0 = \arctan(\frac{R_{\mathrm{JB}}}{L/2})$, x is a variable on the fault length, and z is a variable on the fault depth with probability distribution functions of $p(x)$ and $p(z)$, respectively. These probability distribution functions can be defined somehow to mimic the characteristics of the fault rupture. The term Z_{TOR} for the limits of integral is the depth to the top of a vertical fault rupture with a width of W and a length of L. The variance for the R_{HYP} distance $< R_{\mathrm{HYP}} >_\theta$ can be obtained using the following equation:

$$\sigma^2_{<R_{\mathrm{HYP}}>_\theta} = \int_{z_{\mathrm{TOR}}}^{z_{\mathrm{TOR}}+W}\int_{-L/2}^{L/2}\left[\sqrt{[(R_C^2 + x^2 - 2xR_C\cos(\theta)) + z^2]} - < R_{\mathrm{HYP}} >_\theta\right]^2 p(x)p(z)dxdz. \tag{3}$$

If the azimuth angle of the site is unknown, the variance and the average distance over all virtual sites are estimated by integrating over all possible azimuth angles, which are defined as the following expression:

$$< R_{\mathrm{HYP}} > = \int_0^{2\pi} < R_{\mathrm{HYP}} >_\theta p(\theta)d\theta$$

$$\sigma^2_{<R_{\mathrm{HYP}}>} = \int_0^{2\pi}\int_{Z_{\mathrm{TOR}}}^{Z_{\mathrm{TOR}}+W}\int_{-L/2}^{L/2}\left[\sqrt{[R_C^2 + x^2 - 2xR_C\cos(\theta)) + z^2]} - < R_{\mathrm{HYP}} >_\theta\right]^2 p(x)p(z)p(\theta)dxdzd\theta, \tag{4}$$

in which $< R_{\mathrm{HYP}} >$ is the mean R_{HYP} distance over all azimuth angles, and $p(\theta)$ is the probability distribution of azimuth θ. To obtain the exact function for $p(\theta)$, the JB surface around the fault should be divided into equal segments. Because $p(\theta)$ is a complex function, and it has no close-form solution, we suggest using a simplistic function $p(\theta) = 1/2\pi$ as the probability distribution of azimuth θ in degree. This function slightly underestimates the estimated R_{HYP} distance; however, the result from this simple function converges to the real solution if the segment $d\theta$ is very small. Because the JB surface for vertical strike-slip faults has four identical quarters (see Fig. 1), the integration over θ may be performed for a range of 0 to $\pi/2$ with $p(\theta) = 2\pi$.

The mean R_{HYP} distance (equation 1) can be modified to derive the mean R_{EPI} distance by removing the first integral and z and $p(z)$ terms as follows:

$$< R_{\mathrm{EPI}} >_\theta = \int_{-L/2}^{L/2}\sqrt{[(R_C^2 + x^2 - 2xR_C\cos(\theta))]}p(x)dx. \tag{5}$$

The variance for the R_{EPI} distance can be determined using the following equation:

$$\sigma^2_{<R_{\mathrm{EPI}}>_\theta} = \int_{-L/2}^{L/2}[\sqrt{[(R_C^2 + x^2 - 2xR_C\cos(\theta))]} - < R_{\mathrm{EPI}} >_\theta]^2 \times p(x)dx. \tag{6}$$

Dipping Faults

For a dipping fault with a dip angle of δ, the position of the observation points is located in three different portions of the JB surface, including the lines parallel to the fault length, the quarter-circles, and the lines parallel to the width projection (see Fig. 2). As can be seen in Figure 2, virtual sites around the JB surface of dipping faults can be located on either the hanging wall (HW) or footwall (FW) side. The R_{HYP} distance is different if the sites are located on the HW compared with those located on the FW. The average R_{HYP} distance for a site located on the HW region is less than the average R_{HYP} distance for a site located on the FW region when both sites have the same R_{JB} or R_{HYP} distances. Therefore, the site located on the HW region experiences larger ground motions compared with the other site located on the FW region (Abrahamson and Somerville, 1996; Donahue and Abrahamson, 2014). The mean R_{HYP} distance for a particular azimuth angle of θ, $< R_{\mathrm{HYP}} >_\theta$, is obtained by averaging over all R_{HYP} distances. Thus, the mean R_{HYP} distance is expressed by the following equation:

$$< R_{\mathrm{HYP}} >_\theta = \int_{Z_{\mathrm{TOR}}}^{Z_{\mathrm{TOR}}+W\sin(\delta)}\int_0^{W\cos(\delta)}\int_{-L/2}^{L/2}\sqrt{[(R_C^2 + x^2 - 2xR_C\cos(\theta)) + z^2]}p(x)p(y)p(z)dxdydz, \tag{7}$$

in which x, y, and z are variables on the length, width of the fault surface projection, and the depth of the possible hypocenters, respectively, and $p(x)$, $p(y)$, and $p(z)$ are their probability distribution functions, respectively. The probability distribution functions are defined regarding the characteristics of the given fault rupture. These probability distribution functions can be independent or dependent and even derivable from each other according to the fault characteristics. The boundary conditions for the integrals can be changed based on these characteristics. For instance, if there is any prior information or assumption about the focal depth location, the boundary condition of integral can take into account those assumptions. In equation (7), R_C is an auxiliary distance between the observation point and the middle of the fault length within the width of the fault surface projection that has the possible epicentral point on it and is defined as

$$R_C = \begin{cases} \frac{R_{\mathrm{JB}}+L/2}{\cos(\theta')} & \text{if } 0 \le |\theta| < \theta_1 \\ \sqrt{[y^2 + (L/2)^2] + R_{\mathrm{JB}}^2 - 2R_{\mathrm{JB}}\sqrt{y^2+(L/2)^2}\cos(\gamma)} & \text{if } \theta_1 \le |\theta| < \theta_0 \\ \frac{R_{\mathrm{JB}}+y}{\sin(\theta')} & \text{if } \theta_0 \le |\theta| < 90 \end{cases}, \tag{8}$$

in which

$$\theta_0 = \arctan\left[\frac{\frac{W\cos(\delta)}{2} + R_{\mathrm{JB}}}{L/2}\right]$$

$$\theta_1 = \arctan\left[\frac{W\cos(\delta)/2}{R_{\mathrm{JB}} + L/2}\right]$$

$$\gamma = 180 - \left(\arcsin\left(\frac{\sin(|\theta' - \alpha|)\sqrt{y^2+(L/2)^2}}{R_{\mathrm{JB}}}\right) + |\theta' - \alpha|\right), \tag{9}$$

in which

$$\alpha = \arctan\left[\frac{y}{L/2}\right] \tag{10}$$

and θ' is defined as the angle between a line parallel to the fault length and the line connecting the virtual site and the middle of the fault line within the width of the fault surface projection that has the possible epicentral point on it (see Fig. 2) and is obtained from

$$\theta' = \begin{cases} \arctan\left[\frac{y - \left[\frac{W\cos(\delta)}{2} - \tan(|\theta|)(R_{\mathrm{JB}}+L/2)\right]}{R_{\mathrm{JB}}+L/2}\right] & \text{if } 0 \le \theta < \theta_1 \\ \arctan\left[\frac{R_{\mathrm{Cref}}\sin(\theta) - (\frac{W\cos(\delta)}{2} - y)}{R_{\mathrm{Cref}}\cos(\theta)}\right] & \text{if } \theta_1 \le \theta < \theta_0 \\ \arctan\left[\tan(|\theta|)\left(\frac{y+R_{\mathrm{JB}}}{\frac{W\cos(\delta)}{2}+R_{\mathrm{JB}}}\right)\right] & \text{if } \theta_0 \le \theta < 90 \end{cases}, \tag{11}$$

in which R_{Cref} is the distance between the site and the center of the fault surface projection (see Fig. 2). R_{Cref} can be estimated using equations (8)–(10), assuming $\theta = \theta'$ and $y = W\cos(\delta)/2$.

The variance for the R_{HYP} distance is given by

$$\sigma^2_{<R_{\mathrm{HYP}}>_\theta} = \int_{Z_{\mathrm{TOR}}}^{Z_{\mathrm{TOR}}+W\sin(\delta)} \int_0^{W\cos(\delta)} \int_{-L/2}^{L/2} [\sqrt{[(R_C^2 + x^2 - 2xR_C\cos(\theta)) + z^2]} - < R_{\mathrm{HYP}} >_\theta]^2 \, p(x)p(y)p(z)dxdydz. \tag{12}$$

Finally, if the azimuth of the site is unknown, we average over all possible azimuths as follows:

$$< R_{\mathrm{HYP}} > = \int_0^{2\pi} < R_{\mathrm{HYP}} >_\theta p(\theta)d\theta. \tag{13}$$

Similarly, the variance can be determined using equation (4). Because the JB surface is symmetric along a perpendicular line on the center of fault length, the integration over θ can be done for a range of $-\pi/2$ to $\pi/2$ with $p(\theta) = 1/\pi$.

Similar to the vertical strike-slip fault case, the mean R_{EPI} distance can be derived by removing the first integral and the z and $p(z)$ terms from equation (7). To determine the rupture distance R_{RUP} for a fault with a dip angle of δ and an azimuth angle of θ, the relationships between the R_{RUP} distance and the R_{JB} distance provided by Kaklamanos *et al.* (2011) can be used in equation (7) for the conversion-distance process.

A General Effective Distance-Conversion Equation

The general distance-conversion equations developed in the previous section are independent of the region under study. The problem of employing R_{JB} and R_{RUP} in point-source ground-motion simulations to develop a GMPE is that they can only account for the geometry of the extended-fault rupture model instead of capturing any detailed geological and seismological features (Goda and Atkinson, 2014; Yenier and Atkinson, 2014). Yenier and Atkinson (2014) analyzed earthquake data with moderate-to-large magnitudes from different regions and concluded that if the equivalent point-source model, in which the effective distance (R_{EFF}) is considered as the primary distance metric between a given site and a virtual point which substitutes the whole fault and can mimic the effect of extended-fault rupture source is employed, the apparent source response spectra of those earthquakes can be modeled with a simple far-field Brune point-source model. Thus, the average ground motions for large earthquakes can be acceptably simulated using the equivalent point-source model based on the R_{EFF} distance, even for the sites located at very close distances to the fault rupture.

Using the equivalent point-source model, the extended-fault rupture is subdivided into small elements (subfaults) considered as point sources, and the radiated energy from all subfaults are incoherently added up to compute the GMIM of interest as a measure of energy intensity of shaking at each virtual site. In fact, all subfaults of the extended-fault rupture radiate uniform energy with equal intensity (assuming homogenous energy radiation from the fault). This energy intensity is theoretically proportional to the amplitude of the ground motions captured at the site of interest and decreases with increasing distance, due to spreading over an increasing, either spherical area in a homogeneous whole space, or cylindrical surface in a homogenous half space, as well as scattering and intrinsic absorption (Boore, 2003; Chapman and Godbee, 2012).

Different schemes have been introduced to capture the effects of extended-fault ruptures on distance metrics, GMPEs, or ground-motion simulation approaches (e.g., Singh *et al.*, 1989; Kanamori *et al.*, 1993; Ohno *et al.*, 1993; Andrews, 2001; Boore, 2009). Following the Boore (2009) approach, we use the propagation path function in the frequency domain, which intuitively accounts for the geometrical spreading and anelastic attenuation terms, to construct the effective point-source distance-conversion equation.

The general analytical-based distance-conversion equations, which are calculated based on the uniform weighted average of distances from virtual sites, should be modified to include the effect of geometrical spreading decay and attenuation as suitable weighting factors for the process of distance averaging. In fact, an effective point on an extended-fault rupture should be chosen to give an identical total energy intensity at a given site if this point is compared with an extended-fault rupture. In this regard, the distances from virtual sites to subfaults take appropriate nonuniform weights associated with geometrical spreading and attenuation functions. The following general region-specific distance-conversion equation is developed to estimate effective point-source-based distance metrics (e.g., effective R_{HYP} and R_{EPI} instead of R_{HYP} and R_{EPI}), in place of the extended-fault distance metrics (e.g., R_{JB} and R_{HYP}), which not only accounts for the geometry of the given fault but also considers the effects of the propagation path on radiated seismic waves:

$$G(R_{EFF})\exp\left(\frac{-\pi f R_{EFF}}{Q(f)V_S}\right) = \left[\int_{Z_{TOR}}^{Z_{TOR}+W\sin(\delta)}\int_0^{W\cos(\delta)}\int_{-L/2}^{L/2}\left\{\left[G(\lambda)\times\exp\left(\frac{-\pi\lambda f}{Q(f)V_S}\right)\right]\right\}^2 p(x)p(y)p(z)dxdydz\right]^{0.5}, \quad (14)$$

in which G is the geometrical spreading function, Q, V_S, and f are the quality factor, the shear-wave velocity, and the reference frequency in the attenuation function, respectively. The term λ is the distance between the observation point and possible epicenter or hypocenter locations on the fault, which is defined as

$$\lambda = \sqrt{[(R_C^2 + x^2 - 2xR_C\cos(\theta)) + z^2]}. \quad (15)$$

The R_C is the auxiliary distance, and $p(x)$, $p(y)$, $p(z)$, and $p(\theta)$ are the probability distribution functions, as defined in previous equations. Equation (14) can be simply turned into a summation over the length and width of the fault and the azimuth of the observation points. This equation should be solved with a trial-and-error approach to calculate the R_{EFF} distance.

To determine the R_{EFF} distance for a given reference frequency, a general table for the attenuation term is developed, based on the geometrical spreading and quality factor functions in the region under study and discretized R_{EFF} distances within the range of interest using the left side of equation (14). Then, the triple integration in equation (14) is transferred to summation by discretizing the fault plane into subfaults. The center of each subfault is considered as a possible hypocenter. For a given R_{JB} distance, all distances from the observation point to each subfault, obtained from equation (15), are substituted into the right side of equation (14). The simplified value of the right side of equation (14) gives the resultant effect of anelastic attenuation and geometrical spreading decay terms for a virtual point on the fault that produces the same level of energy intensity as the combination of all subfaults generate at the observation point. Finally, using the developed attenuation table for the left side, the R_{EFF} distance corresponding to the simplified value of the right side is found.

For a given moment magnitude and R_{JB} distance, there is only one point that can be considered as an equivalent point source at a specified source-to-site azimuth. Therefore, the effective distance-conversion approach has no uncertainty for a given azimuth, unlike the general distance-conversion approach according to averaging with uniform weights, in which all points on the fault potentially can be a hypocenter. However, the uncertainty is brought into play for the effective distance-conversion approach through averaging over all azimuth angles around the fault. Of course, this uncertainty is considerably smaller than the uncertainty of the general distance-conversion averaging over all azimuths around the fault.

$$< R_{\mathrm{EFF}} > = \int_0^{2\pi} < R_{\mathrm{EFF}} >_\theta \, p(\theta) d\theta$$
$$\sigma^2_{<R_{\mathrm{EFF}}>} = \int_0^{2\pi} [< R_{\mathrm{EFF}} >_\theta - < R_{\mathrm{EFF}} >]^2 p(\theta) d\theta, \quad (16)$$

in which $< R_{\mathrm{EFF}} >$ is the mean R_{EFF} distance over all possible R_{EFF} distances $< R_{\mathrm{EFF}} >_\theta$.

An Example of Point-Source-Based Distance Conversions

The analytical-based distance-conversion equations that have already been explained are generic and can be used for both shallow and deep earthquakes, small and very large earthquakes, and even for induced earthquakes. Therefore, conversion results depend on the input parameters and their assumptions, such as the geometry of the fault, location of the fault, pattern of possible hypocenters or epicenters on the fault, and the quality factor and geometrical spreading functions of the region of interest. To investigate the effects of using point-source-based distance conversions on ground motions, we select prevalent assumptions about the fault and region and employ them as input parameters in the general distance-conversion equations. These results are based on the assumed input parameters described in the following, and the analyst should modify these parameters according to the characteristics of the fault and the region under study.

The geometry of extended-fault sources is often modeled by a rectangular shape with a width W, a length L, and a dip angle of δ. The rupture width and length of a fault plane are determined based on empirical relationships (e.g., Wells and Coppersmith, 1994; Mai and Beroza, 2000; Somerville *et al.*, 2001; Leonard, 2010, 2012; Somerville, 2014) that are scaled by earthquake magnitude. In this example, we use the global empirical relationships obtained by Wells and Coppersmith (1994). It should be mentioned that the dimensions of simulated faults are much smaller for a given large magnitude if the Somerville *et al.* (2001) relationships, which are derived based on the data from the CEUS, are used.

The next step is to place the fault rupture in a specific location. Earthquake focal depths are assumed to have a nonuniform distribution, such as truncated normal distribution or Weibull distribution (Scherbaum *et al.*, 2004; Mai *et al.*, 2005; Ma and Atkinson, 2006). In this example, we used the results from Scherbaum *et al.* (2004), in which earthquake hypocenter locations are dependent on the moment magnitude and are defined by a truncated normal distribution with a mean hypocentral depth of $h_{\mathrm{avg}} = a + b\mathbf{M}$ in kilometers and a standard deviation of σ, in which the constant values of a, b, and σ are obtained from table I of the Scherbaum *et al.* (2004) study.

This depth distribution and the empirical relationships of Wells and Coppersmith (1994) are consistent because both have been obtained from the same dataset. The estimated hypocentral depth is used to set the center of the fault plane in the simulations. Therefore, the depth to the top of the fault rupture Z_{TOR} can be determined by $Z_{\mathrm{TOR}} = h_{\mathrm{center}} - W/2$, in which h_{center} is the distance from the ground surface to the center of fault plane. Then, possible hypocenters within the simulated fault ruptures are randomly distributed with a uniform distribution along the fault length and width. Those simulated fault ruptures for which the upper edges are extended above the ground surface are shifted down to lie on the surface with a Z_{TOR} of zero. This adjustment reduces the bias in an average sense over many random simulations for the depth of hypocenters, which is used to set the center of the fault plane (Fig. 1).

For the vertical strike-slip fault case in this example, it is assumed that the probability distribution of earthquake hypocenter locations on the fault length and width is uniform; thus, $p(x) = 1/L$ and $p(z) = 1/W$. Similar to the vertical strike-slip fault case, it is assumed that the probability distribution of earthquake hypocenter locations is uniform on the length, depth, and surface projection of the width. Now, the general distance conversion for the case of uniform-weighted average can be used to obtain the converted distance. In this regard, the integration is transferred to summation by discretizing the fault plane. We used 20 subfaults along the length and 20 subfaults along the width of each fault. Thus, there is a total of 400 subfaults for each simulated fault. If the azimuth of the site is unknown, equations (4) and (13) are used to average over all virtual sites around the simulated fault. In this example, virtual sites are located at every two degrees, and the center of each subfault is considered as a possible hypocenter.

Figures 3 and 4 demonstrate the mean converted R_{HYP} and R_{EPI} distances with respect to R_{JB} distances up to 1000 km for a vertical strike-slip fault model and a 50° dip normal fault, respectively, for the selected magnitudes of **M** 5.5, 6.5, and 7.5. The comparison between the mean converted R_{HYP} and R_{EPI} distances for different dip angles demonstrates that the depth distribution of the events and the dip angle of faults control the distance saturation for earthquakes and close site distances.

The R_{HYP} and R_{EPI} distances are always larger than or equal to the R_{JB} distance by an amount ε, which is dependent on the fault size, azimuth angle, and dip angle. Following Scherbaum *et al.* (2004), we define residuals for converted R_{HYP} and R_{EPI} distances $\varepsilon_{\mathrm{HYP}}$ and $\varepsilon_{\mathrm{EPI}}$, respectively, using the following equations:

$$\varepsilon_{\mathrm{HYP}} = R_{\mathrm{HYP}} - \sqrt{R_{\mathrm{JB}}^2 + Z_{\mathrm{TOR}}^2}$$
$$\varepsilon_{\mathrm{EPI}} = R_{\mathrm{EPI}} - R_{\mathrm{JB}}. \quad (17)$$

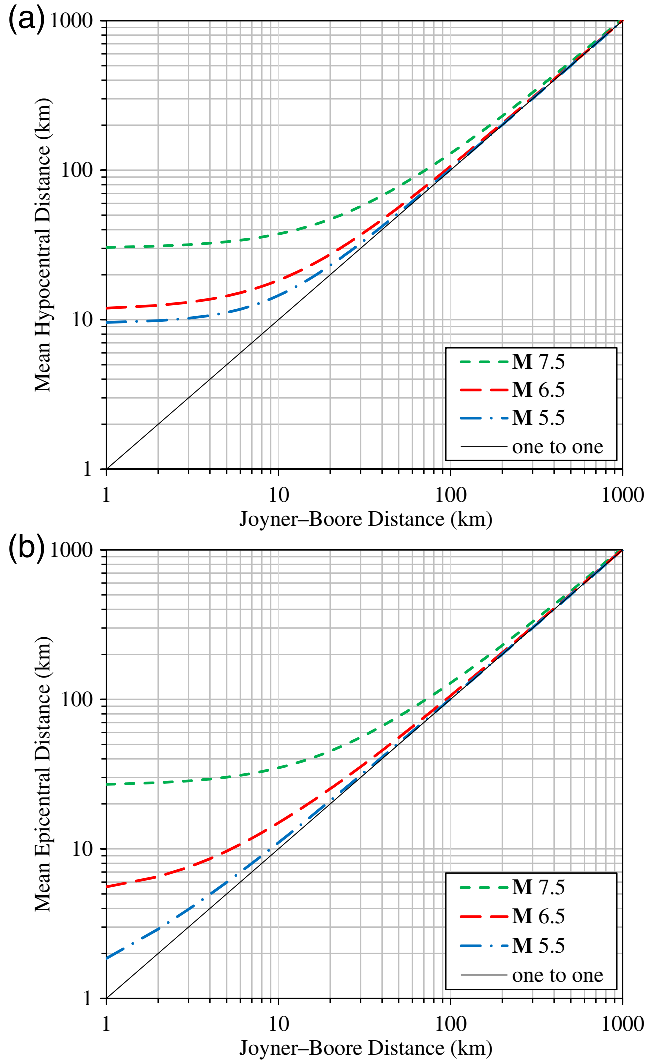

Figure 3. Distance adjustments along a vertical strike-slip fault as a function of JB distance for three selected magnitudes of **M** 5.5, 6.5, and 7.5: (a) hypocentral and (b) epicentral. The color version of this figure is available only in the electronic edition.

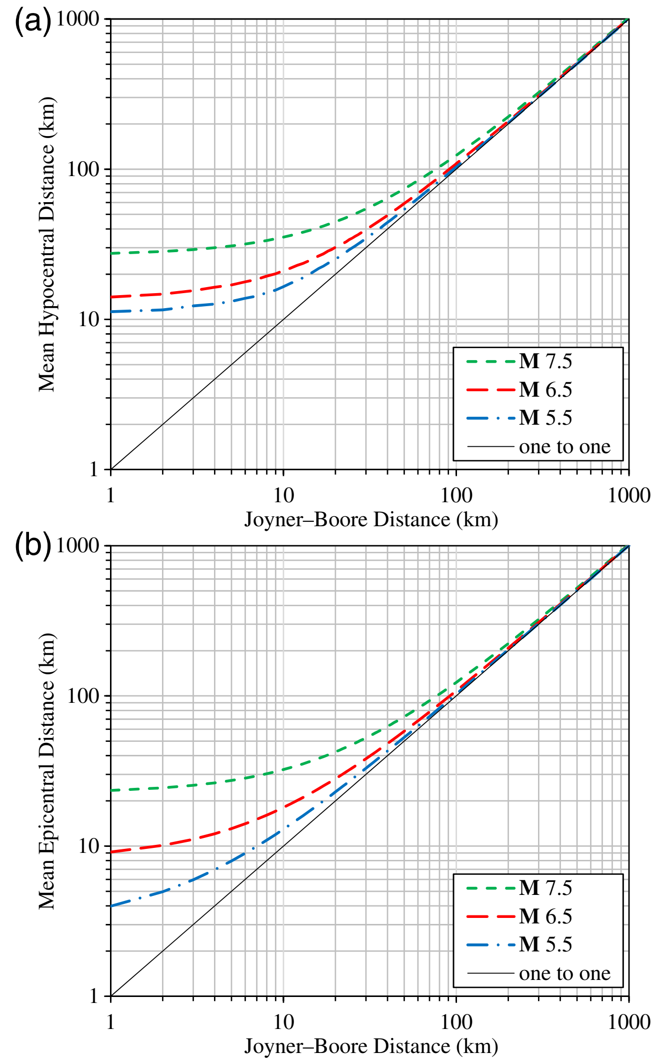

Figure 4. Distance adjustments along a 50° dip normal fault as a function of JB for three selected magnitudes of **M** 5.5, 6.5, and 7.5: (a) hypocentral and (b) epicentral. The color version of this figure is available only in the electronic edition.

Because R_{HYP} and R_{EPI} are always greater than or equal to R_{JB}, residuals and the mean residuals are positive. Figures 5 and 6 show the histogram (frequency) distributions of residuals and the fitted gamma probability distributions for earthquakes with magnitudes of **M** 5.5, 6.5, and 7.5 and an R_{JB} distance of 20 km for vertical and normal faults, respectively. Thus, for a fixed R_{JB} distance and a given magnitude from the example in this section, all possible azimuth angles are considered to obtain the average distance, as shown in these figures. The gamma distribution provides the best fit to the distance residuals because the distribution of the residuals for the virtual site when the azimuth is 0° is uniform, whereas the distribution of the residuals once the azimuth is 90° (the line connecting the virtual site to the center of the fault is perpendicular to the fault line) is exponential. Thus, the combination of these two probability distributions is better captured by a gamma-distributed random variable. The shaping parameters related to the mean and standard deviation of the gamma distribution are derived by fitting the histograms of the residuals (Denker and Woyczynski, 1998). The frequency of residual values shows that the mean and variance of gamma distributions are functions of magnitude and distance. These observations are in good agreement with Scherbaum *et al.* (2004), in which the distance-conversion relationships and residuals are numerically determined using regression analysis on Monte-Carlo-simulated data. These distance conversions are based on the uniform-weighted average of distances from parts of the fault to each observation point.

To estimate the non-uniform-weighted average of distances and to capture the effect of the propagation path on the range of distances, an effective point should be chosen on an extended-fault rupture. To achieve this objective, the point-source-based distance conversions explained previously are modified to incorporate the effect of geometrical spreading

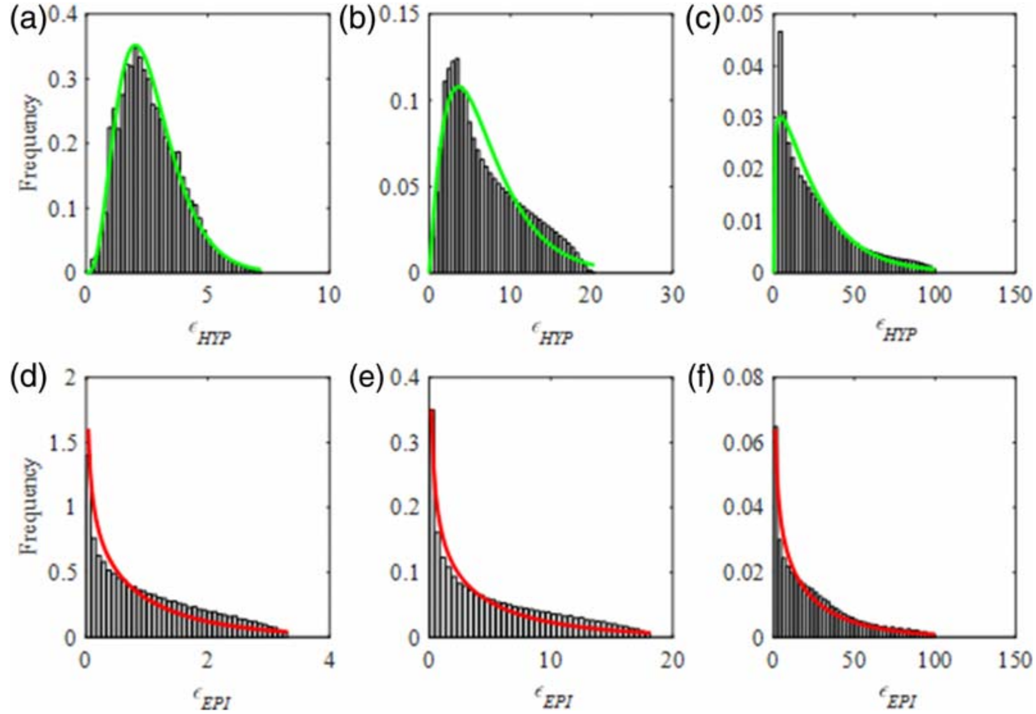

Figure 5. The frequency distribution of residuals fitted by a gamma distribution for a vertical strike-slip fault and an R_{JB} distance of 20 km: (a) hypocentral and **M** 5.5, (b) hypocentral and **M** 6.5, (c) hypocentral and **M** 7.5, (d) epicentral and **M** 5.5, (e) epicentral and **M** 6.5, and (f) epicentral and **M** 7.5. The color version of this figure is available only in the electronic edition.

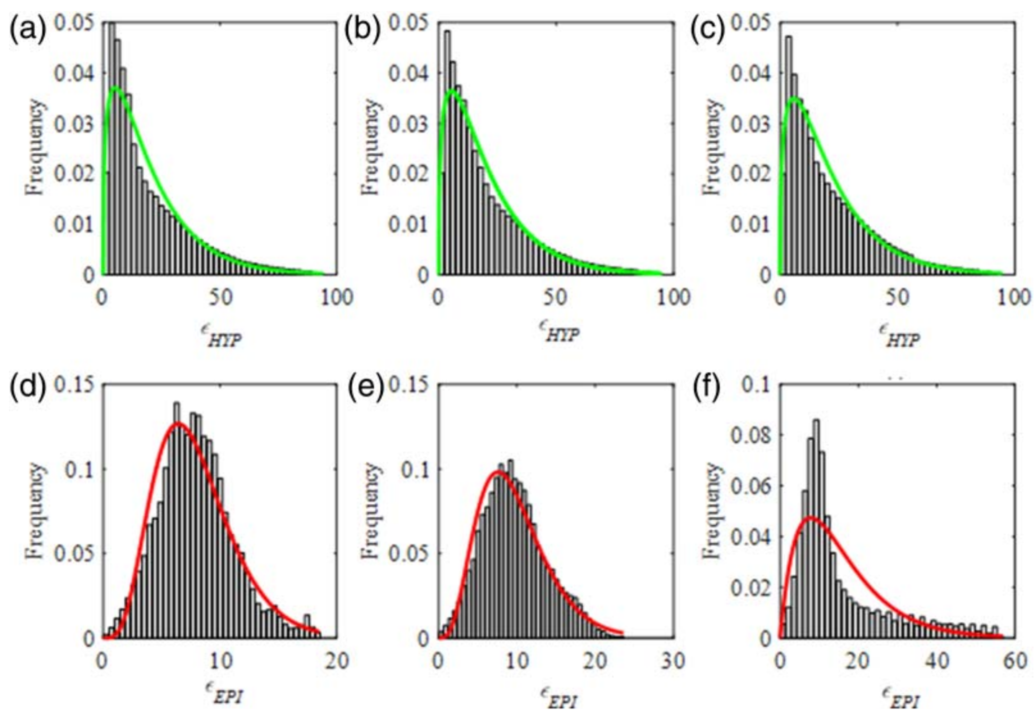

Figure 6. The frequency distribution of residuals fitted by a gamma distribution for a normal 50° dip fault and an R_{JB} distance of 20 km: (a) hypocentral and **M** 5.5, (b) hypocentral and **M** 6.5, (c) hypocentral and **M** 7.5, (d) epicentral and **M** 5.5, (e) epicentral and **M** 6.5, and (f) epicentral and **M** 7.5. The color version of this figure is available only in the electronic edition.

and attenuation functions as weighting factors into the mean distance metrics. To obtain the converted effective distances, geometrical spreading and attenuation functions, as well as the shear-wave velocity and the reference frequency, are required to define the seismological parameters of the region of interest, in addition to previous assumptions about the fault plane.

Far-field body-wave and surface-wave geometrical spreading functions are ideally modeled by $G(R) = R^{-1}$ and $G(R) = R^{-0.5}$ for a whole-space and half-space, respectively (Ou and Herrmann, 1990; Chapman and Godbee, 2012). Some researchers (e.g., Atkinson, 2004; Atkinson and Boore, 2006, 2014) have shown that the geometrical spreading exponent decay for body wave should be higher than R^{-1}, due to the effects of crustal layering and heterogeneities. They indicated that the rate of $R^{-1.3}$ better describes the decay of ground-motion amplitudes with distance for eastern North America. There are some other studies that show the geometric spreading function may be frequency dependent (Frankel, 2015; Sedaghati and Pezeshk, 2016).

The quality factor of $Q = \max(1000, 893f^{0.32})$ and the geometrical spreading function of $G(R) = R^{-1.3}$ for $R < 70$, $R^{+0.2}$ for $70 < R < 140$, and $R^{-0.5}$ for $R > 140$ estimated by Atkinson (2004) for eastern North America are employed in this example to demonstrate the effect of energy decay in the effective distance-conversion equations. These models are consistent with the Pezeshk *et al.* (2011) GMPE because we use this GMPE to show the effect of using effective distance on hazard curves. Further, the crustal shear-wave velocity of $V_S = 3.7$ km/s is used in this example case. The reference frequency of 10 Hz is chosen; however, the distance-conversion results are fairly insensitive to the choice of frequency, which is in good agreement with Boore (2009). The combined effect of geometrical spreading and attenuation functions indicates that the subfaults with shorter distances from the virtual site have higher contribution to the total energy intensity captured at the site than the subfaults with longer distances.

After selecting the appropriate seismological parameters for the region where the site is located, the effective distances are obtained using equation (14) for moment magnitudes of 4.5, 5.0, 5.5, 6.0, 6.5, 7.0, 7.5, and 8.0 and R_{JB} distances of 1, 2, 3, 5, 7, 10, 12, 15, 20, 30, 40, 50, 60, 70, 80, 100, 120, 150, 200, 250, 300, 400, 500, 600, 700, 800, and 1000 km. Again, we use summation instead of integration by discretizing the fault into 20 subfaults along the length and 20 subfaults along the width (400 subfaults in total). Ⓔ Tables S1–S3 (presented in the electronic supplement to this article) tabulate the average effective hypocentral distance for vertical strike-slip faults, 50° dip normal faults, and 40° dip reverse faults, respectively, for this example case. Ⓔ Tables S4–S6 list the average effective epicentral distance for vertical strike-slip faults, 50° dip normal faults, and 40° dip reverse faults, respectively. These magnitude-effective distance-conversion tables are used to convert the extended-fault source-based GMPEs into the point-source-based GMPEs and vice versa, which can be applied for areal seismic sources defined in a PSHA study.

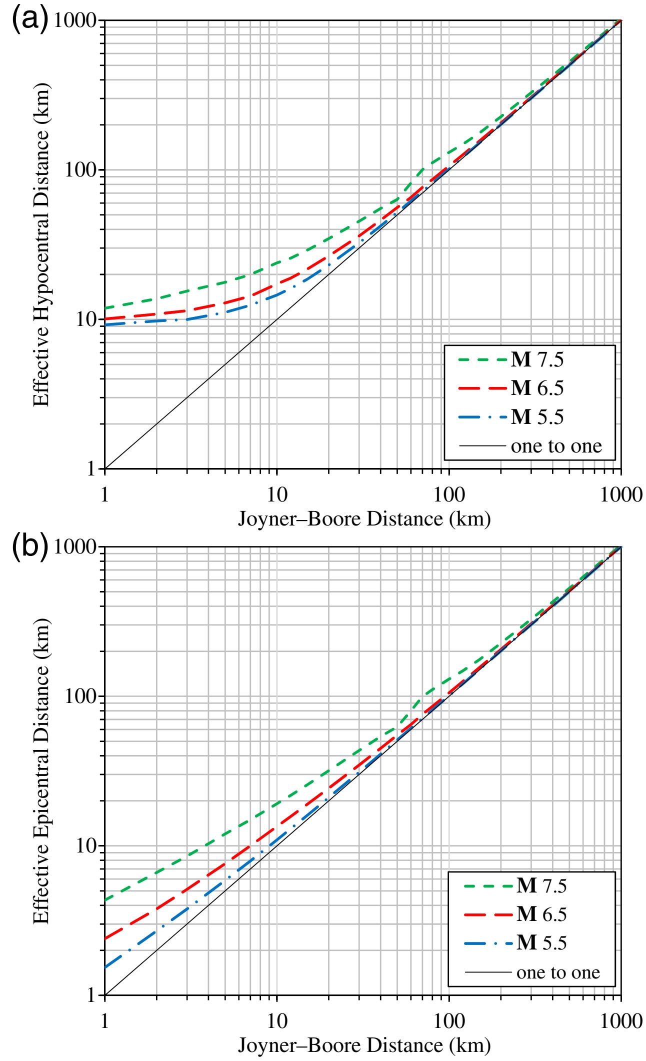

Figure 7. Effective distance adjustments along a vertical strike-slip fault as a function of JB distance for three selected magnitudes of **M** 5.5, 6.5, and 7.5: (a) hypocentral and (b) epicentral. The color version of this figure is available only in the electronic edition.

Figures 7 and 8 illustrate the effective R_{HYP} and R_{EPI} distances averaged over all virtual sites, with respect to R_{JB} distances up to 1000 km for a vertical strike-slip fault model and a 40° dip reverse fault, respectively. The three selected magnitudes of **M** 5.5, 6.5, and 7.5 are used to model the dimension of fault ruptures. In Figures 7 and 8, a direct comparison between the converted effective distances for **M** 5.5, 6.5, and 7.5 is unreasonable because Z_{TOR} for each magnitude is different and is dependent on both the fault-center location and the width of the fault. For instance, in Figure 8, the converted effective distances for **M** 5.5, 6.5, and 7.5 are very similar. In fact, this similarity does not mean that the effective distance for different magnitude should be in the same range, because the depths to the top of the rupture for these magnitudes are ~6.71, 5.11, and 1.53 km, respectively.

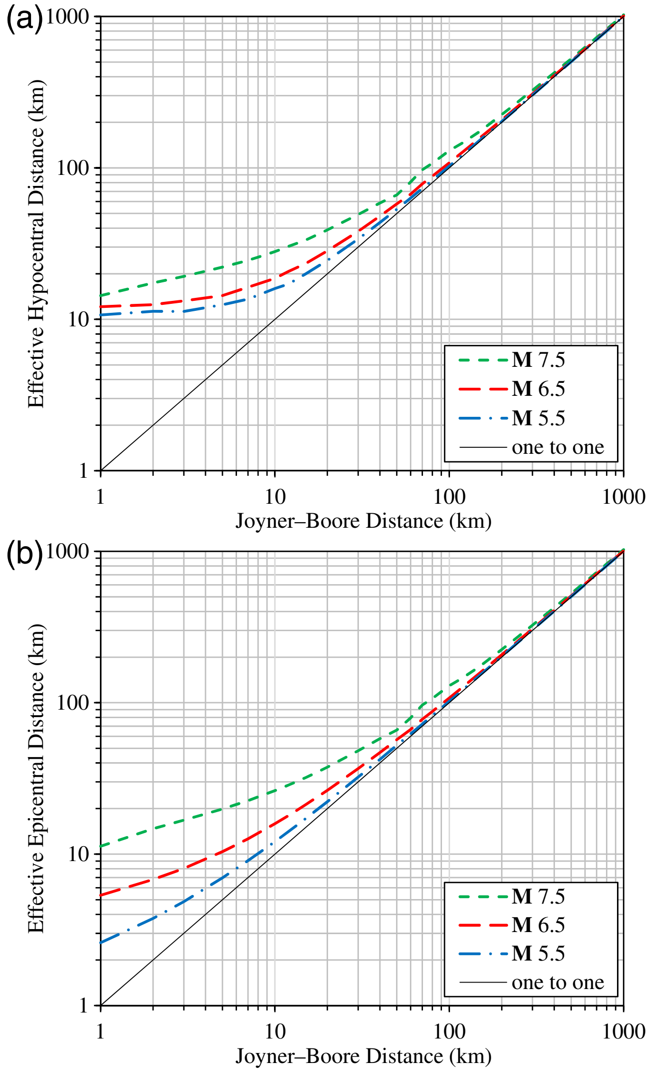

Figure 8. Effective distance adjustments along a 40° dip reverse fault as a function of JB distance for three selected magnitudes of **M** 5.5, 6.5, and 7.5: (a) hypocentral and (b) epicentral. The color version of this figure is available only in the electronic edition.

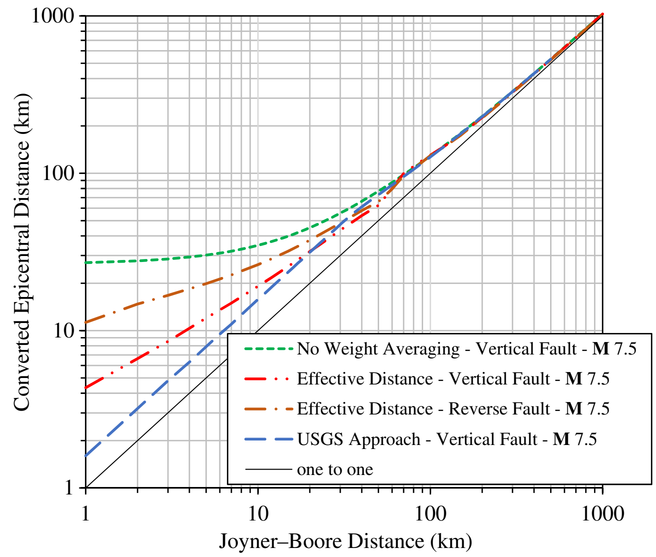

Figure 9. Epicentral distance adjustments along a vertical strike-slip fault and a 40° dip reverse fault as a function of Joyner–Boore distance in kilometers for a magnitude of **M** 7.5. USGS, U.S. Geological Survey. The color version of this figure is available only in the electronic edition.

The plots of distance conversion in Figures 7 and 8 also show a bump around R_{JB} of 50 km, particularly for large magnitudes. This bump is caused by the assumed trilinear geometrical spreading function, in which the middle part is $R^{+0.2}$. For a given fault with **M** 7.5 and R_{JB} of 50 km, the distance from the site to each grid center varies from 50 km to a few hundred kilometers. Thus, incorporating the middle part of the geometrical spreading function into the averaging process leads to estimating higher effective distance. In fact, $R^{+0.2}$ raises the contribution of longer distances compared with $R^{-1.0}$ or $R^{-0.5}$

Comparison of the uniform and non-uniform-weighted average of distances in the conversion process indicates that the distance conversions are dependent upon not only the geometry of fault and the earthquake size but also the geometric spreading of a given region. The non-uniform-weighted averaging on distances lead to increased ground motions at near distances compared with uniform mean distance-conversion approaches.

Comparison with Previous Studies

The effective distances derived from the example for the vertical case are compared with the vertical-fault USGS distance-conversion approach (Petersen *et al.*, 2008) shown in Figure 9. The USGS distance-conversion approach used in the U.S. seismic hazard maps, which only consider the random-ordinated geometry of a vertical fault, is not saturated at close distance, and therefore ground-motion amplitudes monotonically increase with decreasing R_{JB} distance. The USGS approach is also insensitive to the magnitude of earthquakes at close distances. For instance, at an R_{JB} distance of 1 km, the USGS approach results in an R_{EPI} distance of 1.6 km for the three selected magnitudes of **M** 5.5, 6.5, and 7.5, which is inconsistent with the magnitude and distance saturation of ground motions for a large earthquake.

The magnitude and distance saturation of ground motion for a large earthquake indicate that an observation point (or a virtual site) close to a fault can effectively see the closest portions of the extended fault, and most of the fault rupture further away from the site are not involved in the R_{EFF} distance conversion, particularly by increasing magnitude and decreasing the source-to-site distance. Therefore, the effective R_{EPI} distance developed in this study, which is a function of dip angle of a fault and the distance ranges, gives smaller R_{JB} distance values (higher ground-motion amplitudes) than the vertical-fault USGS distance conversion and larger R_{JB} distance values (lower ground-motion amplitudes) than the

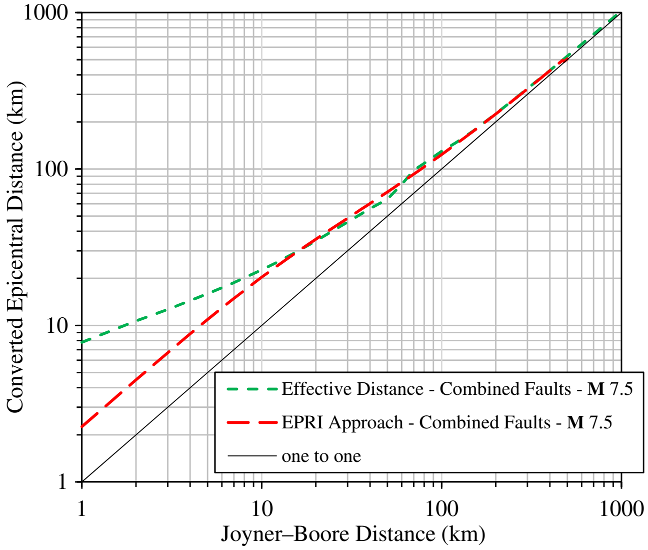

Figure 10. Epicentral distance adjustments along an equal combination of a vertical strike-slip fault and a 40° dip reverse fault as a function of JB distance in kilometers for a magnitude of **M** 7.5. EPRI, Electric Power Research Institute. The color version of this figure is available only in the electronic edition.

mean epicentral distance (Scherbaum *et al.*, 2004) at short distances for the R_{JB}-based GMPEs.

The R_{EFF} distances derived from the example are also compared with the EPRI distance conversion (EPRI, 2004) for the CEUS, as shown in Figure 10. The EPRI (2004) distance-conversion equations are constructed based on the GMPEs developed for the CEUS to partially capture the effect of energy intensity of shaking from a large fault rupture, the random-oriented geometry of a fault to include the effect of unknown fault-rupture models in a specific area, and the Somerville *et al.* (2001) empirical relationship to define the earthquake rupture area. Because the EPRI (2004) distance conversions are developed for a set of GMPEs developed for the CEUS, it may not be appropriate for areas in which regional GMPEs are not available or when different GMPEs and source scaling are assigned to perform PSHA.

The EPRI (2004) approach is also developed for areas in which the orientations of faults are unknown. Thus, there is no specific solution when a specific fault orientation is desired, and the analyst should use the average distance conversion as the final result. Comparison of the vertical and reverse-combined effective distance conversion derived from the example with the EPRI (2004) approach (see Fig. 10) shows that the converted distances for the R_{JB} distances of about 10 km and larger are in good agreement. However, for the near-fault observation points, the magnitude and distance saturation of ground motions for a given large earthquake are not satisfactorily presented in the EPRI (2004) approach, because the earthquake epicenter is assumed to be located at the center of fault (centered epicenters), or the epicenter of an earthquake is uniformly distributed along the length of the rupture (random epicenters).

It is anticipated that the R_{EFF} distance is saturated at very small distances because seismic waves radiated from the small portions of the entire rupture dominate recorded ground motions at the site. Thus, to account for the effects of the magnitude and distance saturation, the impact of the propagation path on seismic waves should be incorporated into the development of distance conversions to obtain the effective points referred to as effective epicenters or effective hypocenters for extended-fault ruptures. These effective points can be used for modeling earthquakes as point sources in PSHA or stochastic ground-motion simulations.

Implications for GMPEs

As stated previously, we developed the analytical-based distance-conversion equations in two phases. In the first phase, the distance-conversion equations were derived to convert between the R_{JB} distance and R_{EPI} or R_{HYP} distances (see equations 1 and 7). These conversion equations can be inverted and used for performing the PSHA study using the empirical-based GMPEs developed based on real observed ground motions. In this case, the distance-conversion equations are used in the empirical-based GMPEs to adjust the distances and to update the total uncertainty accounting for the effect of distance-conversion errors. The mean R_{HYP} or R_{EPI} distances have specific variances that are obtained from equations (3) and (6), respectively. This uncertainty in converted distances must be mapped onto the predicted ground motions due to the laws of error propagation. Using the first-order approximation of the second moment obtained from the Taylor expansion and the derivative of the inverse function, the variance of the inverted mean R_{JB} distance can be calculated as

$$\sigma_{R_{\mathrm{JB}}}^2 = \left[\frac{2\Delta R_{\mathrm{JB}}}{< R >_{R_{\mathrm{JB}}+\Delta R_{\mathrm{JB}}} - < R >_{R_{\mathrm{JB}}-\Delta R_{\mathrm{JB}}}}\right]^2 \sigma_R^2, \qquad (18)$$

in which $< R >_{R_{\mathrm{JB}}+\Delta R_{\mathrm{JB}}}$ can be the normal average or the effective epicentral or hypocentral distances for the input distance of $R_{\mathrm{JB}} + \Delta R_{\mathrm{JB}}$. To propagate the uncertainty of the distance-conversion equations to the ground-motion estimations, we use the following equation:

$$\sigma_{\mathrm{total}} = \sqrt{\sigma_{\mathrm{GMPE}}^2 + \left(\frac{\partial \ln(Y)}{\partial R_{\mathrm{JB}}}\right)^2 \sigma_{R_{\mathrm{JB}}}^2}, \qquad (19)$$

in which σ_{GMPE} is the total standard deviation of the GMPE, $\ln(Y)$ is the natural logarithm of the ground motion, and $\sigma_{R_{\mathrm{JB}}}$ is the standard deviation for the R_{JB}-based GMPEs adjusted for use as the R_{EPI}- or R_{HYP}-based GMPEs (see equation 18). This error propagation issue has been considered and studied in other studies as well, such as EPRI (2004), Scherbaum *et al.* (2004), and Kaklamanos *et al.* (2011).

In the second phase, the effective distance-conversion equation is derived to convert between the R_{EFF} distance and

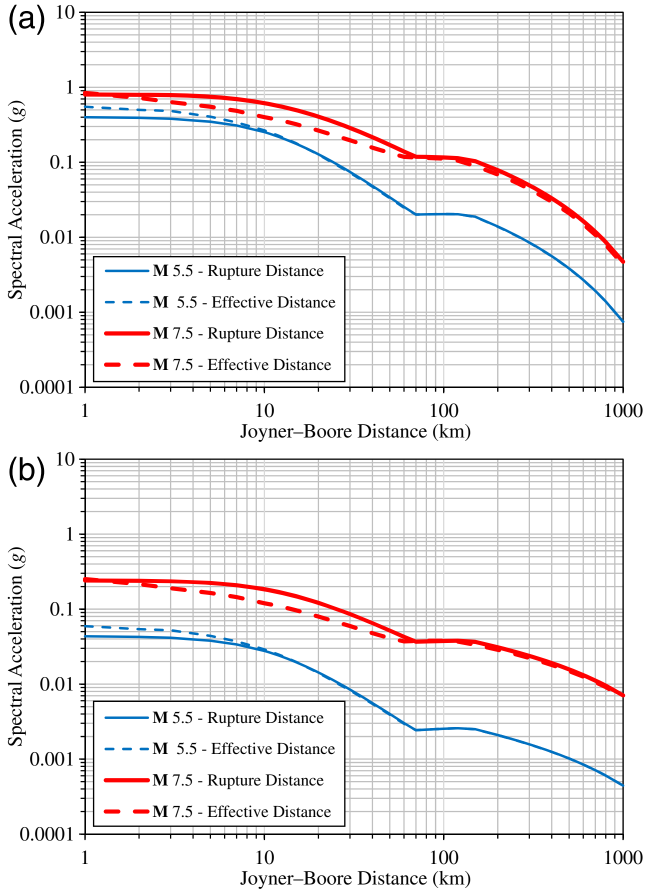

Figure 11. Influence of the effective R_{HYP} distance conversion on a given R_{JB}-based ground-motion prediction equation (GMPE) at a period of (a) 0.2 and (b) 1.0 s. The color version of this figure is available only in the electronic edition.

the R_{JB} distance (see equation 14) for use in the stochastic-based GMPEs, in which the effect of extended-fault source is ignored, or for use in stochastic ground-motion simulations. In these cases, if the azimuth is known, there is no uncertainty for the converted R_{EPI} or R_{HYP} distances because, regarding equation (14), there is only one equivalent point source that can provide the same amount of energy as the whole finite-fault ruptures. Therefore, the total uncertainty remains unchanged. If the azimuth is unknown, the uncertainty is introduced; however, this uncertainty is much smaller than the uncertainty from the first phase. In case of having unknown azimuth, equation (16) can be used in equations (18) and (19) to map the uncertainty of the converted effective R_{EPI} or R_{HYP} distances onto the estimated ground motions.

The R_{EFF} distance can also be used for the development of stochastic-based GMPEs that are obtained directly from the point-source spectrum modeling through the stochastic ground-motion simulation method (Boore, 1983, 2003). The stochastic point-source method is based on an important assumption that the total energy intensity of earthquakes is released from the center point of a postulated fault rupture, and thus the magnitude–distance saturation of ground motions at close distances for large earthquakes are mostly ignored. Ignoring these saturation effects on ground motions from the point-source models may lead us to estimate unrealistically high ground motions at near source-to-site distances compared with the actual extended-fault source models (Boore, 2009; Yenier and Atkinson, 2014).

One way to overcome this problem is to find the effective hypocenters on the fault for each R_{JB} distance using the observation points (virtual sites) around a postulated fault rupture. Then the next step is to use the R_{EFF} distance in the stochastic point-source ground-motion simulation methods to develop stochastic-based GMPEs. Boore (2009) used this approach for a specific simple case study, when the location of a fixed vertical fault and a fixed site are known and earthquakes are uniformly distributed within the fault rupture, to modify the distances used in the point-source-based simulation software (e.g., SMSIM) and to capture the effect of extended-fault source for simulation of ground-motions. Yenier and Atkinson (2014) have also shown that the far-field Brune point-source spectrum can be used within the equivalent point-source approach with effective distance to simulate observed spectra of large (**M** > 6) earthquakes.

The advantage of the general effective distance-conversion equation (see equation 14) developed in this study is that ground motions for large earthquakes generated by extended-source models can be modeled by the equivalent point-source model that incorporates the extended-fault saturation term into the ground-motion simulations for any arbitrary input parameters and functions, such as fault dimensions, location of the fault with respect to virtual sites, probability distribution function of focal depths, and geometrical spreading and anelastic attenuation functions corresponding to the region under study.

Alternative implication for GMPEs is to present the impact of using effective distance conversion on the existing stochastic-based GMPEs in which the effect of extended-fault sources is ignored. Figure 11 illustrates, for example, the impact of using effective R_{HYP} distance conversion for a given suit of R_{HYP}-based GMPE (Pezeshk *et al.*, 2011), which was developed based on a stochastic point-source model (Boore, 2003) for two selected magnitudes of **M** 5.5 and 7.5 and two spectral periods of 0.2 and 1.0 s. The Pezeshk *et al.* (2011) GMPEs, which have been developed for the CEUS, consider the R_{RUP} distance as the distance metric. Therefore, an extra step is required to convert the R_{RUP} distance to the R_{JB} distance and then put the converted R_{JB} distance into the distance-conversion equations. As shown in Figure 11, the discrepancy between ground motions predicted from the R_{RUP}-based GMPE and the effective distance-based GMPE at close distances and large earthquakes is described by the fact that the total energy intensity of ground motions is released within a large fault rupture area, not at a point on the fault. The discrepancy between the effective R_{RUP}- and R_{RUP}-based models increases for a magnitude scenario of **M** 7.5 compared with **M** 5.5. Figure 11

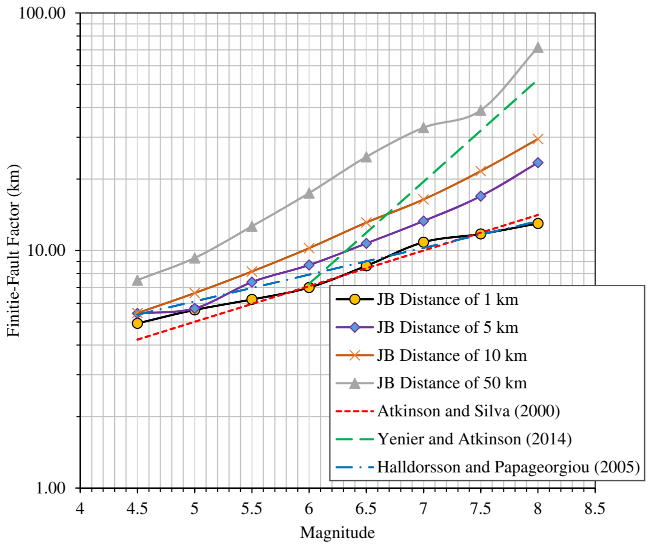

Figure 12. Different models proposed to obtain the finite-fault pseudodepth at a reference distance of 1 km, such as $\log(h) = -0.05 + 0.15\mathbf{M}$ by Atkinson and Silva (2000), $\log(h) = -1.72 + 0.43\mathbf{M}$ by Yenier and Atkinson (2014), and $\ln(h) = -0.515 + 0.259\mathbf{M}$ by Halldorsson and Papageorgiou (2005), as well as the analytical-based finite-fault depth values for different magnitudes at different R_{JB} distances. The color version of this figure is available only in the electronic edition.

also explains that the finite-fault factor h is magnitude and distance dependent. For example, the corrected distance-scaling curve of the GMPE with the effective distance for a magnitude of **M** 5.5 is placed above the uncorrected distance-scaling curve; whereas it comes below the uncorrected distance-scaling curve of the GMPE for a magnitude of **M** 7.5. This implies that the finite-fault factor is lower for lower magnitude, and it increases with increasing magnitude and distance.

Analytical Equation for Finite-Fault Factor

To account for the effects of magnitude and distance saturation at close distances in stochastic point-source simulations or GMPE functional forms, the effective R_{HYP} distance is often connected to the closest distance from the rupture surface as follows:

$$R_{EFF} = \sqrt{R_{RUP}^2 + h^2}, \qquad (20)$$

in which h is known as the finite-fault factor (Boore *et al.*, 2014), equivalent point-source depth, pseudodepth, or fictitious depth (Atkinson and Silva, 2000; Yenier and Atkinson, 2014). For a vertical fault, the rupture distance R_{RUP} is simply expressed as a function of the R_{JB} distance, which is given by

$$R_{RUP} = \sqrt{R_{JB}^2 + Z_{TOR}^2}. \qquad (21)$$

For a given magnitude and R_{JB} distance, Z_{TOR} can be estimated from the dimensions of the fault and the location of

Table 1
Coefficients of the Finite-Fault Depth versus Magnitude and Its Uncertainty

R_{JB}	a	b	σ
1	0.1075	0.1275	0.0210
2	0.0062	0.1513	0.0149
3	−0.0255	0.1600	0.0357
5	−0.1342	0.1825	0.0320
7	−0.1513	0.1901	0.0343
10	−0.2206	0.2076	0.0189
12	−0.2828	0.2198	0.0135
15	−0.2475	0.2197	0.0198
20	−0.2638	0.2287	0.0191
30	−0.3195	0.2468	0.0143
40	−0.3730	0.2643	0.0223
50	−0.3730	0.2706	0.0405

R_{JB}, Joyner–Boore distance.

the fault center. For a vertical strike-slip fault, the effective distance (R_{EFF}) in equation (20) can be obtained from Ⓔ Table S1 for a given magnitude and R_{JB} distance. We developed an analytical-based equation to obtain the finite-fault factor for all magnitudes, ranging from **M** 4.5 to 8 in 0.5-magnitude-unit increments at R_{JB} and the effective R_{HYP} distances tabulated in Ⓔ Table S1.

Different models have been proposed to obtain the finite-fault depth at close distances (Atkinson and Silva, 2000; Halldorsson and Papageorgiou, 2005; Yenier and Atkinson, 2014) from ground-motion databases. These empirical-based models are used to validate the analytical-based model developed in this study. The finite-fault depth is logarithmically modeled as a function of magnitude at a given R_{JB} distance. For example, using equations (20) and (21), the finite-fault factor h for a specified R_{JB} distance is given by the following equation:

$$\log(h) = a + b\mathbf{M}, \qquad (22)$$

with a standard deviation of σ in log 10 units. Table 1 lists all regression coefficients for different R_{JB} distances up to 50 km. However, the model can be prolonged for any arbitrary input parameters and functions corresponding to the region under study. The finite-fault factor indicates that the R_{EFF} distance from a site can never physically be a value less than h.

Figure 12 is a comparison between the analytical-based finite-fault factor obtained in this study with the empirical-based equations proposed by other researchers for different R_{JB} distances. The analytical-based finite-fault factor model at an R_{JB} distance of 1 km is in good agreement with models of Atkinson and Silva (2000) and Halldorsson and Papageorgiou (2005), which are developed based on ground-motion recordings with distances less than 30 km. As shown in this figure, the finite-fault depth model developed in this study not only is magnitude dependent but also is distance dependent. However, at long distances, nonuniform weighting factors approaches uniform weighting factors because the effect of subfaults location on the fault becomes insignificant. Yenier and Atkinson (2014) used data with distances up to 500 km, and thus their proposed model is regressed for all distances, particularly for long distances for which the finite-fault depth is larger. We preferred to model the finite-fault factor versus magnitude at each R_{JB} distance instead of generally regress at all R_{JB} distances. The proposed analytical-based model is derived for a vertical fault with dimensions and seismological parameters explained in the example case. For other dip angles and different tectonic regions, this equation may be varied and can be re-evaluated using equation (14). It should also be mentioned that the finite-fault factor is significantly affected by the azimuth. For instance, for a vertical strike-slip fault, the site located on the middle of the fault has the lowest finite-fault factor for a given R_{JB}, whereas the site located at the ends of the fault has the highest finite-fault factor for the considered R_{JB}. In fact, the results for this example represent an average from all azimuth angles around the fault.

Implication for the PSHA

The impact of using the effective distance on R_{JB}- or R_{RUP}-based GMPEs derived based on the point-source definition is illustrated through a simple PSHA study for a given large areal source. In general, PSHAs are performed using integration over areal sources in which sources are subdivided into small cells as point sources. Delineation of areal seismic sources is often used for the regions with the low-to-moderate seismicity such as CEUS, in which the lack of information on the geometry of active faults is anticipated.

In the PSHA process, the distance between each cell and the site is defined as R_{EPI} or R_{HYP} distances. As stated previously, GMPEs are often developed based on distance metrics such as R_{JB} and R_{RUP} to account for the effects of extended ruptures rather than on distance metrics such as R_{EPI} and R_{HYP} that represent point-source models. The effective distance-conversion equations developed in this study (see equation 14) can be used to estimate the expected GMIM by adjusting a given R_{JB} distance. One way to have consistency between distance metrics used in GMPEs and distance metrics used in the PSHA process for areal seismic sources is to develop a table of effective distance for the pairs of magnitude–JB distance bins using the distance-conversion equations (12) and (14). For example, Ⓔ Table S1 lists the magnitude–R_{EFF} distance pairs for a random-ordinated vertical-fault source of earthquakes at different R_{JB} distances with the assumptions and seismological parameters mentioned previously. To demonstrate the influence of using inconsistent distance metrics on PSHA results at a given site, a circular areal seismic source with a radius of 100 km is considered in which a rock site is located at the center of an areal source similar to the Bommer and Akkar (2012) model. The seismicity of the areal source is assumed to follow a truncated exponential recurrence. For two low- and high-seismicity scenarios, the seismic activity rates are set to 0.5 and 5 events per year, and b-values are set to 1 and 0.85, respectively. The maximum and minimum moment magnitudes are truncated between **M** 5.0 and 8.0, respectively. The R_{RUP}-based GMPEs developed by Pezeshk *et al.* (2011) for the CEUS are applied for these two PSHA scenarios to demonstrate the effects of using inconsistent source-to-site distance metrics on the seismic hazard curves.

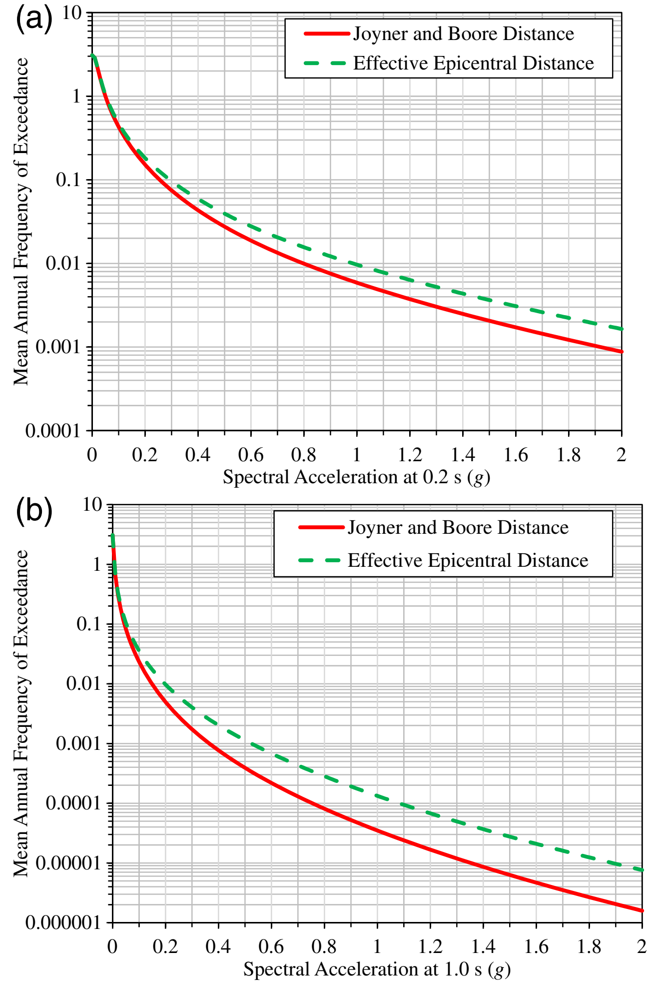

Figure 13. Seismic hazard curves for a rock site at the center of a circular high-seismicity source with a radius of 100 km and for a period of (a) 0.2 and (b) 1.0 s using an R_{JB}-based GMPE. The color version of this figure is available only in the electronic edition.

Figures 13 and 14 depict the effect of using various source-to-site distance metrics on seismic hazard curves at two spectral periods of 0.2 and 1.0 s for the low- and high-seismicity scenarios, respectively. The comparison between seismic hazard curves displays that the effective R_{EPI} distance-metric conversion in GMPEs that are developed based on the R_{JB}- or R_{RUP}-based distance metrics results in significantly higher seismic hazards in PSHA calculations, particularly at the lower probability of exceedance that are often used for the design of significant facilities such as nuclear power plants.

As listed in Ⓔ Tables S1 and S4 for a vertical strike-slip earthquake of magnitude **M** 7.0, the effective R_{HYP} and R_{EPI}

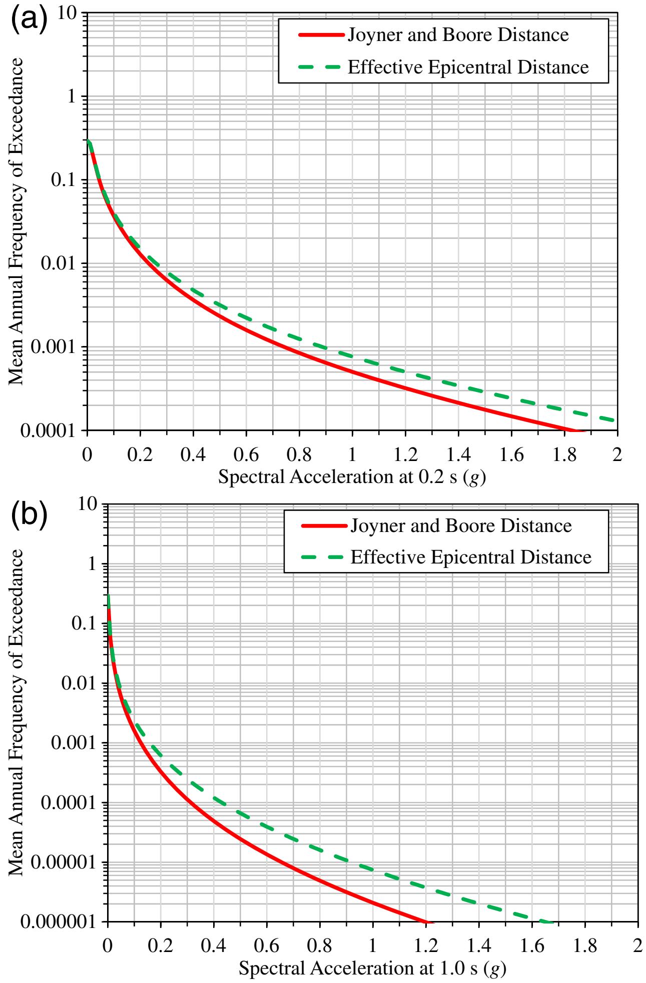

Figure 14. Seismic hazard curves for a rock site at the center of a circular low-seismicity source with a radius of 100 km and for a period of (a) 0.2 and (b) 1.0 s using an R_{JB}-based GMPE. The color version of this figure is available only in the electronic edition.

distance-conversion values for a sample R_{JB} distance of 15 km are about $R_{HYP} = 24.83$ km and $R_{EPI} = 21.67$ km, respectively. In the PSHA study of areal seismic sources, the distance value of 15 km should be considered as an effective R_{HYP} or R_{EPI} distance. The effective R_{HYP} and R_{EPI} distances of 15 km are equivalent to the R_{JB} distance of about 5.5 and 9.5 km, respectively (see Ⓔ Tables S1 and S4) because the R_{JB} distance is always less than or equal to R_{HYP} and R_{EPI} distances. Therefore, for example, if the R_{EPI} distance is used in PSHA, a distance of about 9.5 km should be entered into the fault-source-based GMPE to obtain the adjusted value of R_{JB} distance, which is consistent with the total energy intensity of earthquake on extended-fault sources distributed uniformly within the areal source. The equivalent smaller R_{JB} distances for the epicentral distances in the areal seismic source lead to increasing the seismic hazard results in a PSHA study, particularly at low probability of exceedance and long spectral periods.

The R_{EFF} distance concept explains that it is never possible to place the site on the equivalent point source, and this is exactly what distance saturation means. For instance, if the site is located on the center of the fault, the site sees the effect of many subfaults around itself. Therefore, in areal source hazard calculations, the minimum effective distance does not approach zero, but it saturates with magnitude and distance to capture the effects of radiated seismic waves from different parts of the fault, as well as from the propagation path.

According to the value from these tables, it appears that the denominator of the equation (18) is always larger than the nominator; therefore, the standard deviation of the R_{JB} distance inverted from a given R_{EFF} distance is less than the standard deviation of the converted R_{EFF} distance for a given R_{JB} distance.

Conclusions

In this study, an analytical-based approach is presented to derive source-to-site distance-conversion equations for various distance metrics defined in the published GMPEs. We developed the analytical-based distance-conversion equations in two phases. In the first phase, the distance-conversion equations were derived to convert between the R_{JB} distance and R_{EPI} or R_{HYP} distances (see equations 1 and 7). These conversion equations can be inverted and used for performing the PSHA study using the empirical-based GMPEs developed based on real observed ground motions. In the second phase, the effective distance-conversion equation is derived to convert between the R_{EFF} distance and the R_{JB} distance (see equation 14) for use in the stochastic-based GMPEs, in which the effect of extended-fault source is ignored, or for use in stochastic ground-motion simulations.

The proposed general effective distance-conversion approach is dependent on region-specific material properties, and it can be used not only for random-oriented faults but also for fault ruptures that need to be constrained in strike and dip angles, based on the tectonic and geologic features in areal sources. In contrast with the EPRI and USGS approaches, JB surface with a given R_{JB} distance is defined for virtual sites around an extended-fault rupture, and then the converted R_{EPI} and R_{HYP} distances are derived analytically using the law of sines and cosines. The distance-conversion process can also be combined with region-specific geometrical spreading and attenuation functions to convert the resultant point-source distance metrics into new effective R_{EPI} or R_{HYP} distance metrics that may be used in PSHA and equivalent point-source ground-motion simulations to account for the effect of extended-fault sources near the sites.

The R_{EFF} distances, which capture both effects of the extended-fault source and the wave propagation path on ground motions, indicate that the same amount of energy intensity should be captured at the virtual site, relative to the entire fault rupture during a large-magnitude earthquake. The following steps are required to determine the general effective distance conversion developed in this study for use in the PSHA studies and the equivalent point-source ground-motion simulations:

- define the size of rectangular fault plane of width W and length L, with respect to magnitude, using the source scaling law (e.g., Wells and Coppersmith; 1994; Somerville *et al.*, 2001);
- define the probability distribution function for the focal depth (e.g., truncated normal distribution and Weibull distribution) and then the location of the fault in depth;
- define the fault dip angle and constrain the fault strike, based on the tectonic and geologic information;
- define region-specific geometrical spreading and attenuation functions, based on the seismological parameters obtained for the region of interest;
- determine the effective distance using equation (14) for a given reference frequency, and then develop magnitude-effective distance pairs (distance conversion) in a table; and
- use the table of distance conversion in the PSHA study for areal seismic sources, in which earthquakes are modeled as epicenters or hypocenters, and in the equivalent point-source model to simulate strong ground motions.

Use of empirical distance conversions such as those proposed by EPRI (2004) and Scherbaum *et al.* (2004) simply breaks down for earthquake epicenters close to the site, where the site is located within a given areal seismic source that is likely to dominate the contribution to hazard, particularly for low annual frequencies of exceedance. The general effective distance-conversion approach developed in this study overcomes this limitation by defining the effective epicenters or hypocenters. The effective distances do not approach zero and saturate with magnitude and distance to capture the effects of radiated seismic waves from different parts of the fault as well as the propagation path.

As stated previously, the USGS distance-conversion results are applicable only for the vertical fault ruptures. In this study (see Fig. 9), comparison between a dipping fault and a vertical fault indicates that the dipping fault source model with a surface projection of fault at the ground surface predicts a longer effective distance (a lower intensity of shaking) than the vertical fault source model in which the earthquake is uniformly distributed along the line projection of fault relative to the surface projection of fault at the ground surface. The effective distance-conversion equation proposed in this study is generic and can be used for shallow and deep earthquakes, small and very large earthquakes, and even induced earthquakes.

Induced earthquakes are also of small magnitudes at shallower depths than the range of magnitudes and depths of tectonic earthquakes that are covered by published GMPEs. Using the R_{JB}-based GMPEs relative to point-source-based GMPEs in the PSHA study to capture the ground motions for the induced events may lead to reduction of predicted motions at short distances to a given site.

Data and Resources

No data were used in this article. Most of the analyses were performed using the MATLAB R2015a release (www.mathworks.com/products/matlab, last accessed December 2015). Some plots were also made using MATLAB.

Acknowledgments

The authors would like to thank Karen Assatourians, Mark Stirling, Thomas Pratt, and an anonymous reviewer for their thoughtful comments and constructive suggestions that significantly improved this article. This project was partially supported by the Tennessee Department of Transportation.

References

Abrahamson, N. A., and P. G. Somerville (1996). Effects of the hanging wall and footwall on ground motions recorded during the Northridge earthquake, *Bull. Seismol. Soc. Am.* **86,** 93–99.

Andrews, D. J. (2001). A suggestion for fitting ground-motion attenuation near an extended earthquake source, *Seismol. Res. Lett.* **72,** 454–461.

Atkinson, G. (2004). Empirical attenuation of ground motion spectral amplitudes in southeastern Canada and the northeastern United States, *Bull. Seismol. Soc. Am.* **94,** 1079–1095.

Atkinson, G. M., and D. M. Boore (2006). Earthquake ground-motion prediction equations for eastern North America, *Bull. Seismol. Soc. Am.* **96,** no. 6, 2181–2205.

Atkinson, G. M., and D. M. Boore (2014). The attenuation of Fourier amplitudes for rock sites in eastern North America, *Bull. Seismol. Soc. Am.* **104,** no. 1, 513–528.

Atkinson, G. M., and W. Silva (2000). Stochastic modeling of California ground motions, *Bull. Seismol. Soc. Am.* **90,** no. 2, 255–274.

Bommer, J. J., and S. Akkar (2012). Consistent source-to-site distance metrics in ground-motion prediction equations and seismic source models for PSHA, *Earthq. Spectra* **28,** 1–15.

Boore, D. (1983). Stochastic simulation of high-frequency ground motions based on seismological models of the radiated spectra, *Bull. Seismol. Soc. Am.* **73,** 1865–1894.

Boore, D. M. (2003). Simulation of ground motion using the stochastic method, *Pure Appl. Geophys.* **160,** 635–676.

Boore, D. M. (2009). Comparing stochastic point-source and finite-source ground-motion simulations: SMSIM and EXSIM, *Bull. Seismol. Soc. Am.* **99,** 3202–3216.

Boore, D. M., C. Di Alessandro, and N. A. Abrahamson (2014). A generalization of the double-corner-frequency source spectral model and its use in the SCEC BBP validation exercise, *Bull. Seismol. Soc. Am.* **104,** no. 5, 2387–2398.

Chapman, M. C., and R. W. Godbee (2012). Modeling geometrical spreading and the relative amplitudes of vertical and horizontal high frequency ground motions in eastern North America, *Bull. Seismol. Soc. Am.* **102,** 1957–1975.

Denker, M., and W. A. Woyczynski (1998). *Introductory Statistics and Random Phenomena*, Birkhauser, Boston, Massachusetts.

Donahue, J. L., and N. A. Abrahamson (2014). Simulation-based hanging wall effects model, *Earthq. Spectra* **30,** 1269–1284.

Electric Power Research Institute (EPRI) (2004). *CEUS Ground Motion Project: Final report, EPRI Report 1009684*, Electric Power Research Institute, Palo Alto, California.

Frankel, A. (2015). Decay of S-wave amplitudes with distance for earthquakes in the Charlevoix, Quebec, area: Effects of radiation pattern and directivity, *Bull. Seismol. Soc. Am.* **105,** 850–857.

Goda, K., and G. M. Atkinson (2014). Variation of source-to-site distance for megathrust subduction earthquakes: effects on ground motion prediction equations, *Earthq. Spectra* **30,** 845–866.

Halldorsson, B., and A. S. Papageorgiou (2005). Calibration of the specific barrier model to earthquakes of different tectonic regions, *Bull. Seismol. Soc. Am.* **95,** 1276–1300.

Kaklamanos, J., L. G. Baise, and D. M. Boore (2011). Estimating unknown input parameters when implementing the NGA ground-motion prediction equations in engineering practice, *Earthq. Spectra* **27,** 1219–1235.

Kanamori, H., J. Mori, E. Hauksson, T. Heaton, L. K. Hutton, and L. M. Jones (1993). Determination of earthquake energy release and M_L using TERRAscope, *Bull. Seismol. Soc. Am.* **83,** 330–346.

Leonard, M. (2010). Earthquake fault scaling: Self-consistent relating of rupture length, width, average displacement, and moment release, *Bull. Seismol. Soc. Am.* **100,** no. 5A, 1971–1988.

Leonard, M. (2012). Earthquake fault scaling: Self-consistent relating of rupture length, width, average displacement, and moment release, *Bull. Seismol. Soc. Am.* **102,** no. 6, 2797.

Ma, S., and G. Atkinson (2006). Focal depth distribution for earthquakes with $m_N \geq 2.8$ in western Quebec, southern Ontario and northern New York, *Bull. Seismol. Soc. Am.* **96,** 609–623.

Mai, P. M., and G. C. Beroza (2000). Source scaling properties from finite-fault-rupture models, *Bull. Seismol. Soc. Am.* **90,** no. 3, 604–615.

Mai, P. M., P. Spudich, and J. Boatwright (2005). Hypocenter locations in finite-source rupture models, *Bull. Seismol. Soc. Am.* **95,** 965–980.

Ohno, S., T. Ohta, T. Ikeura, and M. Takemura (1993). Revision of attenuation formula considering the effect of fault size to evaluate strong motion spectra in near field, *Tectonophysics* **218,** 69–81.

Ou, G.-B., and R. B. Herrmann (1990). Estimation theory for strong ground motion, *Seismol. Res. Lett.* **61,** 99–107

Petersen, M. D., A. D. Frankel, S. C. Harmsen, C. S. Mueller, K. M. Haller, R. L. Wheeler, R. L. Wesson, Y. Zeng, O. S. Boyd, D. M. Perkins, *et al.* (2008). Documentation for the 2008 update of the United States national seismic hazard maps, *U.S. Geol. Surv. Open-File Rept. 2008–1128*, 1–128.

Pezeshk, S., A. Zandieh, and B. Tavakoli (2011). Hybrid empirical ground-motion prediction equations for eastern North America using NGA models and updated seismological parameters, *Bull. Seismol. Soc. Am.* **101,** 1859–1870.

Scherbaum, F., J. Schmedes, and F. Cotton (2004). On the conversion of source-to-site distance measures for extended earthquake source models, *Bull. Seismol. Soc. Am.* **94,** no. 3, 1053–1069.

Sedaghati, F., and S. Pezeshk (2016). Estimation of the coda-wave attenuation and geometrical spreading in the New Madrid seismic zone, *Bull. Seismol. Soc. Am.* **106,** no. 4, 1482–1498.

Singh, S. K., M. Ordaz, J. G. Anderson, M. Rodriguez, R. Quaas, E. Mena, and D. Almora (1989). Analysis of near-source strong-motion recordings along the Mexican subduction zone, *Bull. Seismol. Soc. Am.* **79,** 1697–1717.

Somerville, P. (2014). Scaling relations between seismic moment and rupture area of earthquakes in stable continental regions, *PEER Report, 2014/14*, 1–48.

Somerville, P. G., N. Collins, N. A. Abrahamson, R. Graves, and C. K. Saikia (2001). Ground motion attenuation relations for the central and eastern United States, *Report to U.S. Geol. Surv. Open-File Rept., NEHRP External Research Program, Award No. 99–HQ–GR–0098*.

Wells, D. L., and K. J. Coppersmith (1994). New empirical relationships among magnitude, rupture length, rupture width, rupture area, and surface displacement, *Bull. Seismol. Soc. Am.* **84,** 974–1002.

Yenier, E., and G. M. Atkinson (2014). Equivalent point-source modeling of moderate-to-large magnitude earthquakes and associated ground-motion saturation effects, *Bull. Seismol. Soc. Am.* **104,** no. 3, 1458–1478.

Bechtel Corporation
50 Beale Street
San Francisco, California 94105
btavakol@bechtel.com
(B.T.)

Department of Civil Engineering
The University of Memphis
3815 Central Avenue
Memphis, Tennessee 38152
fsdghati@memphis.edu
spezeshk@memphis.edu
(F.S., S.P.)

Manuscript received 7 June 2017;
Published Online 13 February 2018